Taphonomic pathway of exceptionally preserved fossils in the Lower Ordovician of Morocco

Farid Saleh, Bernard Pittet, Pierre Sansjofre, Pierre Gueriau, Stefan Lalonde, Jean-Philippe Perrillat, Muriel Vidal, Victoire Lucas, Khadija El Hariri, Khaoula Kouraiss, et al.

Journal Pre-proof

Taphonomic pathway of exceptionally preserved fossils in the Lower Ordovician of Morocco

Farid Saleh Bernard Pittet Pierre Sansjofre Pierre Guériau Stefan Lalonde Jean-Philippe Perrillat Muriel Vidal Victoire Lucas Khadija El Hariri Khaoula Kouraiss Bertrand Lefebvre

PII: S0016-6995(20)30029-2

DOI: https://doi.org/doi:10.1016/j.geobios.2020.04.001

Reference: GEOBIO 904

To appear in: *Geobios*

Received Date: 6 February 2020

Revised Date: 27 February 2020

Accepted Date: 3 April 2020

Please cite this article as: Saleh, F., Pittet, B., Sansjofre, P., Guériau, P., Lalonde, S., Perrillat, J.-P., Vidal, M., Lucas, V., Hariri, K.E., Kouraiss, K., Lefebvre, B.,Taphonomic pathway of exceptionally preserved fossils in the Lower Ordovician of Morocco, *Geobios* (2020), doi: https://doi.org/10.1016/j.geobios.2020.04.001

Taphonomic pathway of exceptionally preserved fossils in the Lower Ordovician of Morocco ✡

Farid Saleh [a,*], Bernard Pittet [a], Pierre Sansjofre [b], Pierre Guériau [c], Stefan Lalonde [d], Jean-Philippe Perrillat [a], Muriel Vidal [d], Victoire Lucas [a], Khadija El Hariri [e], Khaoula Kouraiss [e], Bertrand Lefebvre [a]

[a] Univ. Lyon, Université Claude Bernard Lyon 1, ENS de Lyon, CNRS, UMR 5276 Laboratoire de Géologie de Lyon : Terre, Planètes, Environnement, F-69622 Villeurbanne, France

[b] MNHN, Sorbonne Université, CNRS UMR 7590, IRD, Institut de minéralogie, des Matériaux et de Cosmochimie, Paris, France

[c] Institute of Earth Sciences, University of Lausanne, Géopolis, CH-1015 Lausanne, Switzerland

[d] Univ. Brest, CNRS, IUEM Institut Universitaire Européen de la Mer, UMR 6538 Laboratoire Géosciences Océan, Place Nicolas Copernic, 29280, Plouzané, France

[e] Département des Sciences de la Terre, Faculté des Sciences et Techniques, Université Cadi-Ayyad, BP 549, 40000 Marrakesh, Morocco

* Corresponding author. E-mail address: farid.saleh@univ-lyon1.fr (F. Saleh).

✡ Corresponding editor: Emmanuel Fara.

Abstract

The Fezouata Shale in Morocco is the only Lower Ordovician *Lagerstätte* to yield a diverse exceptionally preserved marine fauna. Sediments of this formation have yielded soft to lightly

sclerotized taxa that were previously unknown from the Ordovician. Yet the taphonomic pathway of fossils from this formation remains poorly understood. Here, based on drill core material, a close association between exceptional preservation and a specific sedimentary facies is evidenced in the Fezouata Shale. This facies corresponds to calm sea-bottoms, sporadically smothered by distal storm deposits. The patterns of exceptional preservation in this facies indicate that most animals were dead and decayed on the seafloor prior to their burial by distal storm deposits. Furthermore, contrasted elemental and molecular compositions between fresh-cored and altered materials show that surface deposits of the Fezouata Shale were substantially affected by recent weathering. This weathering resulted in the leaching of organic materials from fossils originally preserved as carbonaceous compressions and the transformation of pyrite into iron oxides. Understanding the processes behind the current patterns of soft tissue preservation in the Fezouata Shale is essential prior to any paleontological description, especially of taxa with no current representatives.

Keywords:

Depositional environment

Sedimentary facies

Lagerstätten

Fezouata Shale

Mineralization

1. Introduction

Konservat-Lagerstätten have revolutionized our understanding of metazoan evolution and diversification, owing to the preservation in these deposits of soft-bodied and lightly sclerotized organisms that normally are not preserved (Caron et al., 2006, 2010; Smith and Caron, 2010; Gutiérrez-Marco and García-Bellido, 2015; Lerosey-Aubril et al., 2017; Knaust and Desrochers, 2019). These deposits are particularly abundant in Cambrian Series 2 and 3, providing critical insights into the Cambrian Explosion, one major pulse in animal evolution (Butterfield, 1995; Liu et al., 2008; Zhang et al., 2008; Duan et al., 2014; Lei et al., 2014). The younger Fezouata Biota (late Tremadocian) was discovered in the early 2000s in the Central Anti-Atlas of Morocco, and is the only Lower Ordovician *Lagerstätte* to yield a diverse exceptionally preserved fauna *(*Van Roy et al., 2010, 2015a), providing key information on the transition between the Cambrian and Ordovician (Lefebvre

et al., 2016). Anatomical information found in fossils from this deposit is critical for deciphering the evolution of major animal phyla (Vinther et al., 2008, 2017; Van Roy et al., 2015b; Lefebvre et al., 2019).

The general depositional environment of the Fezouata Shale is constrained, and is storm-dominated with an indirect influence of tides (Martin et al., 2016; Vaucher et al., 2017). The processes behind the formation of sedimentary structures related to this environment were explained in recent works (Vaucher et al., 2016, 2017). Two types of exceptional preservation have been documented in the Fezouata Shale: the first one occurs in concretions (Gaines et al., 2012a). This type of preservation requires vigorous sulfate reduction around carcasses, resulting in the establishment of prominent chemical gradients around dead animals and leading to the early precipitation of minerals around non-biomineralized tissues (Gaines et al., 2012a). The other type of preservation is associated with shale (Martin et al., 2016). In these levels, fossils occur exclusively at bed junctions and not within beds (Vaucher et al., 2016, 2017), strongly supporting the view that organisms were smothered on the seafloor under a new blanket of distal storm deposits, rather than having been carried in sediment flows (Saleh et al., 2018).

However, the step-by-step mechanism behind this type of preservation remains largely unexplored. Most fossils collected in shales are preserved as molds or imprints on the sediments (Martin et al., 2016), but it is unclear whether these organisms were originally preserved as carbonaceous compressions. Other non-biomineralized tissues, such as trilobite digestive tracts and echinoderm water-vascular systems, are preserved in 3D red to orange iron oxides (Gutiérrez-Marco et al., 2017; Lefebvre et al., 2019). Considering that numerous diagenetic mechanisms may alter the original anatomy of fossil organisms over geological time, deciphering the taphonomic processes at play in the Fezouata Shale is essential for palaeontological interpretations, especially for taxa without extant representatives. Consequently, the aim of this study is to provide insights into soft tissue taphonomy in the Fezouata Shale based on a detailed sedimentological investigation constraining the facies in which exceptional preservation occurred, in addition to a careful geochemical analysis deciphering the mechanism leading to the current patterns of preservation in this facies.

2. Geological context

During the Ediacaran (600 Ma), the Panafrican Orogeny led to the formation of the Gondwana supercontinent. Gondwana extended from the South Pole to intermediate latitudes in the Northern Hemisphere. A rifting phase took place in its western part at the end of the Cambrian. At the beginning of the Ordovician, a long-term transgression resulted in the flooding of Gondwanan margins by epicontinental seas (Destombes et al., 1985). The entire Lower Ordovician succession in the Zagora region in Morocco was deposited in a generally shallow environment at high latitude, close to the

palaeo-South pole (Torsvik and Cocks, 2011, 2013; Fig. 1(A)). These deposits unconformably overlie middle to upper Cambrian strata and are separated by an unconformity from the overlying lower to middle Darriwilian (Middle Ordovician) deposits of the Tachilla Fm. (Choubert, 1952; Destombes et al., 1985). The Fezouata Shale (Tremadocian–Floian) consists of blue-green to yellow-green sandy mudstones and siltstones that coarsen upwards. They are up to 900 m thick in the Zagora region (Vaucher et al., 2016). The long-term transgression at the beginning of the Ordovician was followed by a regression leading to the deposition of massive dark brown sandstones characteristic of the Zini Fm. (late Floian) above the Fezouata Shale (Martin et al., 2016). The Lower Ordovician succession was interpreted to have been deposited in a storm-wave dominated sedimentary environment (Martin et al., 2016) indirectly influenced by tides (Vaucher et al., 2017). The corresponding palaeoenvironments range from the foreshore (S-SE) to the upper offshore (N-NW) (Vaucher et al., 2017). In intermediate settings of the Ternata plain, the Bou Izargane locality (Fig. 1(B)), studied in the present work, has yielded abundant exceptionally preserved fossils including lightly cuticularized arthropods, sponges, and soft parts of echinoderms (Van Roy et al., 2015a; Botting, 2016; Lefebvre et al., 2019). This locality (Fig. 2) exposes part of the lower interval with exceptional preservation, dated as late Tremadocian (*Araneograptus murrayi* graptolite Zone; Lefebvre et al., 2018).

3. Material and methods

3.1. Field work

In February 2018, a 6.5 m core was drilled at the top of the Bou Izargane section (30°30'00.5" N; 5°50'56.7" W; Fig. 2: core 1), in the Ternata plain, *ca*.18.5 km N of Zagora (Morocco), and a second 6.7 m core (Fig. 2: core 2) was made 6.8 m below the first one to cover most of the sedimentary succession in this locality. Both cores are temporally stored at the University of Brest, France. The outcrop in this locality was logged and highly excavated in 2014 and yielded hundreds of exceptionally preserved fossils, registered in the collections of the Cadi-Ayyad University, Marrakesh.

3.2. Sediment preparation and analyses

The cores were cut and scanned, using a core XRF-scanner, for major elements (Si, Al, K) expressed as oxides (wt% SiO_2, Al_2O_3 and K_2O) at the University of Brest, France. Then, they were described for their lithology, grain size, depositional sedimentary structures, and bioturbation intensity and size, and drawn on a 1:1 scale at the Laboratoire de Géologie de Lyon, France. The uppermost 2 m of each core are extremely weathered and show the same greenish color as on the outcrop. The lower, fresher portions of the cores range from dark grey to black in color. Twelve thin sections were

made from the cores. Transect analyses combined into elemental maps (Table S1, Appendix A) from both green and black core sediments were made on nine samples using a Bruker M4 Tornado micro-XRF instrument operating at 50 kV, 600 μA. This mapping of the major elements was done to better visualize discrete lithological changes in the facies and to determine the composition of silty to very fine sand grains (Fig. 3). In addition, around 100 Raman spectra were collected from nine core specimens (Table S1, Appendix A) using a Labram HR800 - Jobin Yvon Horiba spectrometer equipped with semi-confocal optics at the University of Lyon, France. A microscope with a ×100 objective was used to focus the excitation laser beam, 532 nm exciting line, on a 1-3 μm size spot and to collect the Raman signal in the backscattered direction. Acquisitions were performed using two accumulations of 30 s and a laser power of about 5 mW on the sample surface.

3.3. Statistical approach

Cores give precise information in terms of sedimentary facies and their evolution, but only minimal information on the vertical occurrences of exceptionally preserved fossils. Conversely, field and hand sample observations made at Bou Izargane provide important information on the occurrence of exceptional preservation, but with unprecise information on the facies in which exceptional preservation occurred, due to surface weathering. Thus, the stratigraphic sequence from the core was compared to the field-based sequence logged along the same section and described by Vaucher et al. (2016; Fig. 4(A, B)). Cores were made starting at the upper surface of the outcrop from which the original log was made. For more precision, correlations between cores and outcrop were made based on comparisons of facies defined in Vaucher et al. (2017) and in the present study (Table 1). Using this correlation, a statistical approach was developed to link these two distinct, though complementary sets of data gathered from outcrops (i.e., occurrences of exceptional preservation) and from drill cores (i.e., detailed sedimentary facies).

The obtained 13.2 m-thick core succession was divided into 22 60 cm-thick successive intervals. Then, the proportion of each sedimentary facies identified was calculated in these intervals. A Principal Component Analysis (PCA) was performed to identify the facies accounting for the largest variance between the 22 intervals (Hammer et al., 2001). Facies that are homogeneously distributed are less likely to explain discrepancies in occurrences of exceptionally preserved fossils and therefore were removed from further statistical analysis. The facies exhibiting the highest dissimilarity (i.e., with the largest variance) were selected for a Classical (hierarchical) Cluster Analysis (CCA). CCA allows investigating the heterogeneities in terms of sedimentary facies between the 22 intervals by separating them into clusters (Hammer et al., 2001). Vertical alternation of intervals between the clusters was plotted against the pattern of soft tissue preservation in the field to check any direct link between the sedimentary facies and exceptional fossil preservation. Then, a

Similarity Percentage analysis (SIMPER; Hammer et al., 2001) was made to identify which facies caused the highest dissimilarity between these clusters and thus, to decipher the correlation of different facies with the absence/presence of exceptional preservation. Finally, a student t-test was applied to investigate whether the difference in the proportions of facies causing the dissimilarity between clusters was significant.

3.4. Fossil analyses

Twenty fossil specimens (Table S1, Appendix A) collected from late Tremadocian localities in the Zagora area, Morocco, and registered in the paleontological collections of the Cadi-Ayyad University, Marrakesh, Morocco (acronym: AA), Lyon 1 University, Villeurbanne, France (UCBL-FSL) and the Musée des Confluences, Lyon (ML), were included in this study. Some of these fossils were analyzed using a FEI Quanta 250 scanning electron microscope (SEM) equipped with backscattered and secondary electron detectors in addition to an energy-dispersive X-ray analyzer (EDX) operating at accelerating voltages ranging from 5 to 15 kV. At low energies, light elements such as C can be detected, while at higher energies, detection of heavier elements is optimized. Some samples were analyzed using a synchrotron beam X-ray fluorescence at the DIFABBS beamline at the Soleil synchrotron, Paris, France, in order to determine the minor-to-trace elemental composition of the fossils, as well as of the surrounding matrix.

4. Results

4.1. Core description

Both cores are dominated by Si-rich (Fig. 3(A)), quartz dominated (Fig. 4(A)), normally graded beds having an erosive base (Figs. 3(A), 4(A)). The thickness of these beds varies from 0.2 to 2.5 cm. Intervals with finer grains exist between these beds (Figs. 3(A), 4(A)); these levels are Al- and K-rich (Fig. 3(A)) and are likely more argillaceous (Fig. 4(A)). Mn and Co are present around and within the layers with the coarsest grains especially in greenish sediments (Fig. 5). The coarsest layers bear wavy laminations. These wavy layers are hummocky cross stratifications (HCS) with a centimeter- to decimeter-scale estimated wavelength (Figs. 3, 5), as also observed on outcrops (Vaucher et al., 2017). Occasionally, these HCS are associated with Ca-rich deposits (Figs. 3, 5). The distribution of Fe in the cores positively correlates with the general distribution of both Al and K (Fig. 3(A)). In fresh and lightly altered sediments, Fe correlates with S as well (Fig. 3), when pyrite is present (Fig. 4(B)). This pyrite is generally surrounded by a halo of C-rich organic material (Figs. 4(B), 6). An absence of both pyrite and C is evidenced in surface sediments that are extensively altered (Fig. 6). Fe-rich minerals in these recently weathered sediments are iron oxides.

Evidence for bioturbation is abundant in the cores (Figs. 3, 5). Bioturbation is mainly horizontal (i.e., less than 1-2 cm in depth). Some escape burrows have been observed in coarse-grained layers (Fig. 3(A)). Only one 5-cm vertical bioturbation occurs in the uppermost part of the sedimentary succession. A detailed mm-scale description of the two combined drill cores is given in Fig. 7.

4.2. Facies identification

Five sedimentological facies are defined from the core and are designated herein as Fc1 to Fc5. Fc1 is the finest grained facies (Fig. 8(A)); it is homogeneous and mostly composed of argillaceous material (Fig. 9(A)). Fc2 contains coarser siliciclastic layers (Fig. 9(B)) showing a normal grading with a considerable amount of fine sediments in between (Fig. 9(B)). Sediments in Fc3 are coarser than in Fc2 (Fig. 8(A)). Fc3 consists of stacked, normally graded layers with little to no fine-grained sediments in between, and in rare occasions some small HCS are present (see Vaucher et al., 2016, 2017 for direct evidence for HCS; Fig. 9(C)). Fc4 is made of coarser sediments than in Fc3 (Fig. 8(A)) and contains abundant wavy laminations (HCS; Fig. 9(D, E)). Fc5 consists of coarse siltstones (Fig. 8(A)) containing sometimes Ca-rich deposits (Fig. 9(F)).

The increase of quartz (SiO_2) and decrease of clays (K_2O and Al_2O_3) from Fc1 to Fc5 is shown in Fig. 8(B). Bioturbation is mostly present in Fc2, Fc3, Fc4, and Fc5 (Fig. 9) and may vary in intensity within the same facies (Fig. 9(D, E)). Pyrite occurs mainly in Fc2, Fc3, Fc4, and Fc5, with the largest pyrite crystals being observed in Fc2 (Fig. 9(B)).

4.3. Statistical analyzes

Principal component analysis shows that most of the variance between the 22 defined intervals is related to Fc2, Fc3, and Fc4 (Fig. 10(A)). Fc1 and Fc5 can be excluded from further statistical tests because they contribute to less than 5% of heterogeneities between intervals. Based on variations in the proportion of Fc2, Fc3, and Fc4 in the 22 intervals, two clusters were extracted (Fig. 10(B)). The alternation of intervals between Cluster 1 and Cluster 2 fits with 95% fidelity the presence/absence of exceptional preservation in these deposits, validating that this type of preservation is directly linked to the sedimentary facies in the Fezouata Shale (Fig. 10(D)).

Fc2 and Fc4 are responsible for 81% of the difference between the two clusters (Fig. 10(C)). Fc2 is abundant in Cluster 1 (Fig. 10(C)) which is correlated with intervals bearing exceptional preservation (Fig. 10(D)). Fc4 is abundant in Cluster 2 (Fig. 10(C)) that is correlated with intervals where exceptional preservation is absent (Fig. 10(D)). The differences in the distribution of Fc2 and

Fc4 in Cluster 1 and Cluster 2 are significant ($p = 0.003$ and $p = 2.8.10^{-7}$, respectively). The difference in the proportion of Fc3 between the two clusters is not significant ($p = 0.1$), indicating that this facies did not significantly contribute to the differences observed between intervals with and without exceptional preservation.

4.4. Fossil preservation

Red/orange 3D fossils from the Bou Izargane locality appear to be preserved in iron oxides (Fig. 11(A)). In these samples, iron is present in two different morphologies: abundant in small euhedral crystals (Fig. 12(B, C)), and dispersed as framboid-shaped minerals (Fig. 12(D)). The obtained SEM spectra, at low voltage, show a low concentration of C in these fossils (Fig. 11(A)) in comparison with the abundance of C around pyrite in fresh deposits (Figs. 4(B), 6). C is abundantly present in fresh sediments (Fig. 6) but absent in cuticularized to lightly sclerotized fossils preserved as 2D imprints as well (Fig. 11(B)). In both 3D and 2D modes of preservation, thin star-like (Fig. 12(E, G)) iron-rich minerals (Fig. 12(H)) may cover parts of the fossils. The majority of this Fe in star-shaped minerals is found in fossils that are covered by Co and Mn-rich deposits (Fig. 13) in rose-like minerals (Fig. 12(F, G)).

5. Discussion

5.1. General depositional environment

The increase in SiO_2 and decrease of Al_2O_3 and K_2O from Fc1 to Fc5 (Fig. 8; Table S2, Appendix A) is indicative of the energy at which sediments were deposited. In open marine environments, Si-rich sandstones (i.e., quartz) are found in high-energy proximal settings, while Al- and K-rich clays are generally found in lower energy, more distal environments. In the Fezouata Shale, Si is associated with the coarsest grained sediments (Figs. 3, 5) originating from the shallowest settings (i.e., beach to the SE of Zagora; Vaucher et al., 2017). In this sense, the finest grained sediments (Figs. 3, 5) belong to more distal settings and are K- and Al-rich. The dominant clay mineral in this formation is illite (Saleh et al., 2019). The presence of oscillatory structures in Fc4 and Fc5 (Fig. 9) and the absence of these structures in other facies support this interpretation. HCS are sedimentary structures first described as characteristic of storm deposits (Harms et al., 1975). Wave oscillation induces wave orbitals in the water column that decrease in size with depth. In a shallow environment, wave orbitals form large HCS on the seafloor (Vaucher et al., 2016, 2017). Conversely, in deep environments, these orbitals dissipate before attaining the sediment and thus leave no trace on the seafloor. Furthermore, the abundance of normally graded beds in the core (Figs. 3(A), 4(A)) indicates that sediment was deposited by successive events of decreasing energy. These event beds can

be formed either during storms or turbiditic events. In the Fezouata Shale, the monotonous alternation of event beds with the background sedimentation and the occurrence of HCS favor the interpretation of event sediments as storm deposits. In this sense, the high frequency of storm events is another indication of less distal sites, more affected by storm wave oscillations (Vaucher et al., 2016). The absence of event layers in Fc1 (Fig. 9(A)) indicates that this facies is characteristic of settings below the Storm Wave Base (SWB). Fc2 shows some event beds isolated in the background sedimentation and an absence of HCS (Fig. 9(B)). This facies is characteristic of settings below the SWB, but more proximal than Fc1. Fc3, showing stacked storm events, and rarely HCS (Fig. 9(C)), is more proximal than Fc2. Fc3 was deposited around the SWB. In Fc4, HCS are abundantly present (Fig. 9(D, E)), revealing a more proximal environment above the SWB with higher energy than what is observed in Fc3. The coarse grains constituting Fc5 (Fig. 9(F)) and the presence of HCS with a wavelength estimated to be around 10 cm were deposited closer to the Fair Weather Base (FWB). Due to the coarse-grained and high porosity of Fc5, elemental enrichment (e.g., Mn; Fig. 5) may occur and alter the original elemental distribution of this facies (Fan et al., 1992). The Ca-rich deposits in some laminae (Figs. 3(A, C), 5) may resemble carbonate cement deposited in deep settings (i.e., basin) of some Cambrian *Lagerstätten* (Gaines et al., 2012b). Carbonate cements are used to explain the presence of exceptional preservation in some deposits due to their ability to block exchange between sediments and the water column thus depriving oxidants of attaining dead carcasses (Gaines et al., 2012b). However, critical differences exist between these cements and the observed carbonate laminae in the Fezouata Shale. Carbonate cements from the Cambrian are deposited at the top of turbiditic events (Gaines et al., 2012b), while in the Fezouata Shale, Ca-rich deposits occur only at the base of oscillatory structures with a coarse lithology and a high porosity (Figs. 3(A, C), 5). If carbonate precipitation occurred in the Fezouata Shale, its original Ca source must be the bioclasts observed in thin sections cutting through the bottom of storm deposits (Fig. 4(C)) especially because carbonates are not evidenced elsewhere in this formation (Vaucher et al., 2016). Thus, the most distal facies is Fc1 and the most proximal facies is Fc5 with Fc2, Fc3, and Fc4 in between, respectively. This model of facies is in accordance with outcrop-based sedimentological models for the Fezouata Shale from which an outcrop to cores correlation was made (Table 1).

5.2. Facies for exceptional preservation

Exceptional preservation requires burial by event deposits (Vaucher et al., 2016). In the Fezouata Shale, this condition was present in the entire core (Fig. 10(D)) except in Fc1 that constitutes only 6% of the studied deposits (Fig. 7). Another requirement for exceptional fossil pyritization is iron availability. Iron was a limited element in the Fezouata Shale environment (Saleh et al., 2019). In these deposits, Fe supply was likely associated to periods with high seasonality leading to high iron-

rich continental fluxes to the sea (Saleh et al., 2019) (Fig. 10(D)). Thus, during intervals with enhanced Fe availability exceptional preservation could occur in intervals I-4, I-5, I-6, I-7, I-12, I-13, I-14, I-20, I-21, and I-22 (Saleh et al., 2019; Fig. 10(D)).

Although the general conditions for exceptional preservation were occurring in many intervals, the presence of exceptionally preserved fossils at Bou Izargane is more restricted (i.e., exceptional preservation occurred in I-4, I-5, I-6, I-7, I-13 and I-20; Fig. 10(D)). Thus, the absence of soft parts, e.g., in I-14, is possibly related to the original absence of living organisms on the sea floor. This hypothesis is confirmed by the absence of benthic fauna (both hard and soft parts) in this interval, showing that environmental conditions on surface sediments were probably not favorable for the colonization of this environment (Saleh et al., 2018). Statistical analyses show that an alternation of clusters, which are reconstructed based on the proportion of different sedimentary facies, can predict with a 95% fidelity the presence and location of intervals with exceptional preservation discovered in the field (Fig. 10(D)). Levels with higher proportions of Fc2 and lower proportions of Fc4 have a higher potential to yield exceptional preservation (Fig. 10(C)). This is because Fc2 combines rather calm environmental conditions with lower energy events compared to other facies, allowing living organisms to colonize the sea floor (Saleh et al., 2018), in addition to burial during event deposition, a prerequisite condition for exceptional preservation (Vaucher et al., 2017).

The unique negative correlation between the alternation of clusters and the patterns of exceptional preservation is exemplified in I-10 (Fig. 10(D)). I-10 yielded a considerable number of mineralized skeletons (Saleh et al., 2019). The absence of exceptional preservation in this facies does not result from the original absence of living organisms, but may be due to the lack of berthierine in this level (Saleh et al., 2019). Berthierine is an iron-rich clay mineral that can be deposited in the sediments from a primary clay precursor under anoxic conditions (Tang et al., 2017). It is documented in most intervals with exceptional preservation in the Cambrian (Anderson et al., 2018), and only in specific levels of the Fezouata Shale in which exceptional preservation occurred (Saleh et al., 2019). In experimental studies, it was shown that berthierine slows down bacterial decay due to the damage of bacterial cells (McMahon et al., 2016). However, some authors interpreted its presence as a symptom of the same conditions that led to exceptional fossilization, rather than a cause for soft tissue preservation (Anderson et al., 2018). In order to further investigate this discrepancy, future work should study the timing of berthierine formation and its exact geographical distribution in consecutive sediment laminae.

5.3. Taphonomic pathway of fossils in Fc2

5.3.1. Burial and decay

In the Fezouata Shale, fossils were preserved *in situ* (Vaucher et al., 2017; Saleh et al., 2018) in Fc2 (Fig. 14(E)). Fc2 combines a fine grain size and the occurrence of event deposits favoring burial. Both conditions are necessary for exceptional preservation (Gaines et al., 2012b). However, in distal settings comparable to Fc2, burial occurred only during strong storms (Saleh et al., 2018), causing a delay in the start of the fossilization process. For instance, in one interval with exceptional preservation 600 fossils were discovered, but only a limited number of them show soft tissue preservation (about 30 stylophorans, 10 trilobites, and 5 marrellomorphs; Lefebvre et al., 2019). Furthermore, the single preserved hyolithid specimen with soft parts from the Fezouata Shale shows totally decayed tentacles (Martí Mus, 2016). These two examples of soft tissue preservation suggest that organisms were most probably dead and decaying on the sea floor prior to their burial (Fig. 14(A-C)). Pre-burial decay was also used to explain the absence of completely cellular animals (i.e., without cuticle, sclerites, or minerals) from the Fezouata Shale (Saleh et al., 2020) in contrast to most Cambrian *Lagerstätten.* In the Cambrian, soft-bodied and lightly sclerotized organisms were killed during obrution events and transported by the same event to another facies for their preservation leading to a smaller exposure to pre-burial decay (Gaines, 2014). This taphonomic process can explain the abundance of soft cellular animals and hyolithid tentacles in sites such as the Burgess Shale (Moysiuk et al., 2017; Saleh et al., 2020).

5.3.2. Authigenic mineralization

Experimental approaches have shown that pyrite can form under different circumstances (Rickard and Luther, 1997; Grimes et al., 2002). Pyrite can precipitate in the water column, surface sediments and even under deep burial under anoxic conditions. However, selected soft anatomies replicated by pyrite minerals are often associated with active, localized sulfate reduction in iron-rich pore waters during early diagenesis resulting in a strong concentration gradient, and confining pyrite precipitation to dead carcasses (Farrell, 2014). Under sulfate-reducing conditions, bacteria transform organic matter and sulfates into HS^- and then to hydrogen sulfides H_2S, which react with Fe in a series of reactions to form pyrite (Raiswell et al., 1993; Schiffbauer et al., 2014). In the Fezouata Shale, anoxic conditions leading to sulfate reduction were established at the time of burial at the bottom of storm deposits (Vaucher et al., 2016, 2017) leading to pyritization of some tissues deposited under event beds. The chemical stress generated by oxygen depletion in the sediment is also evidenced by horizontal biological traces that are shallow with some escape burrows crossing event deposits. As bioturbation depth is minimal, it is most probable that the sediment was anoxic a few centimeters below storm deposits. Further ichnological work should investigate biological traces in detail in order to test this scenario and constrain oxygenation between the bottom of the water column and the sediments.

Because in open marine environments sulfates are not limited, pyritized tissues are those providing sufficient organic material to form H_2S (Jørgensen, 1982; Jørgensen et al., 2019; Fig. 14(D)). Laboratory experiments made under surface-sediment conditions have shown that the most labile decaying soft parts produce considerable amounts of H_2S, which reacts with iron to form nuclei for pyrite framboids (Butler and Rickard, 2000). However, less labile soft parts produce less H_2S, and thus fewer nuclei leading to the precipitation of mainly cubic, and sometimes octahedral minerals (Gabbott et al., 2004). In the Fezouata Shale, framboid minerals in 3D fossils are scarce (Fig. 12(D)) and much less abundant than euhedral pyrite (Fig. 12(C)); this emphasizes the removal of a considerable quantity of organic material, due to burial delay and oxic decay, prior to the permissive chemical conditions for pyrite precipitation. If a tissue did not provide sufficient H_2S to form nuclei when anoxic conditions occur (e.g., non-cellular cuticles made of polysaccharides) for neither euhedral nor framboidal minerals, it remains preserved as a carbonaceous compression.

5.3.3. Late diagenesis, metamorphism, and modern weathering

Although mineralogical and chemical evidences favor the idea of an early authigenic pyritization of some soft tissues in the Fezouata Shale, the geochemical signal of these minerals in fossils from outcrops is clearly altered. The absence of S-rich minerals in surface fossils (Fig. 11) indicates that pyrite was oxidized and S was partly leached after early diagenesis (Ahm et al., 2017). This can be due to either metamorphism or modern weathering. According to mineral distributions in shales from the Fezouata *Lagerstätte*, sediments did not experience high burial temperatures as only 3 km of sediments were deposited above the Fezouata Shale (Ruiz et al., 2008; Saleh et al., 2019; Fig. 14(F)). This is confirmed by a Raman signature representative of fresh organic matter (i.e., low burial temperatures around 200°C) characterized by the presence of the D4 band and the absence of the D2 band, as well as by the higher intensity of the D1 band compared to the G band (Rahl et al., 2005; Kouketsu et al., 2014; Fig. 6). These temperatures are lower than in other deposits with soft tissue preservation in which the D4 band is less pronounced and the G band has a higher intensity than the D1 band (Topper et al., 2018). Thus, it is more likely that the removal of S from pyrite in green surface sedimentary rocks of the Fezouata Shale results from modern weathering rather than from metamorphism. In the Draa Valley, this formation is exposed to abundant water circulations, as revealed by the numerous abandoned terraces near the outcrops and by the abundance of water wells in the area (Warner et al., 2013). Fast pyrite oxidation may be induced by Mn-oxides that are abundant in circulating waters in arid environments with occasional rain similar to the Draa Valley (Potter and Rossman, 1979; Warner et al., 2013). Depending on Mn-oxide quantities in circulating waters, the outcome of pyrite oxidation may differ. When the quantity of Mn-oxide is high enough to fully oxidize pyrite, the resulting products of this reaction are Fe-oxides and Mn-sulfates (Larsen and

Postma, 1997). Additionally, since manganese oxides are much stronger adsorbents of elements such as Co and Ni than iron oxides (McKenzie, 1980), the reduction of manganese oxide may cause a major release of these elements in the surrounding environment (Postma, 1985). If the quantities of Mn-oxides are not sufficient to fully oxidize pyrite, pyrite oxidation by H_2O molecules and atmospheric O_2 will take place and unleash considerable amounts of sulfates, thus reducing the pH of the environment and contributing to the dissolution of nearby carbonates (Larsen and Postma, 1997). In the Fezouata Shale, it seems that both pyrite oxidation pathways were operational. Mn-oxides altered pyrite, contributing to the initial precipitation of Co- and Mn-rich deposits. The latter reaction may lead to a diffusion of Mn in the sediments, which would explain the distribution of Mn around the appendages of the analyzed marrellomorph (Richard et al., 2013; Fig. 13). Subsequently, H_2O transformed the remaining pyrite into Fe-oxides and sulfuric acid, and was also responsible for the dissolution of Ca (Lucas, 2019) and the poor preservation of skeletal elements of different groups with preserved soft parts, such as echinoderms (Lefebvre et al., 2019).

5.3.4. Original mode of preservation and comparison with the Chengjiang Biota

The contrast between the presence of C in fresh sediments (Figs. 4(B), 6) and its absence from surface deposits (Fig. 6) may be also the result of modern weathering. The association of C to pyrite crystals in fresh sediments (Fig. 4(B)) suggests that the original mode of preservation in the Fezouata Shale includes both carbonaceous compressions and pyrite replicates. In this sense, flattened fossils (Fig. 11(B)) were most probably originally preserved as 2D carbonaceous films. However, due to recent weathering, C was leached from originally non-pyritized structures and pyrite was transformed to iron oxides in 3D mineralized tissues (Fig. 14(G)). Similarities in terms of taphonomic pathway of soft tissues in the Fezouata Shale are particularly high with the Chengjiang Biota. Early studies of the Chengjiang Biota have emphasized the role of pyrite in replicating some tissues within individual fossils (Gabbott et al., 2004; Zhu et al., 2005). Later works focusing on less weathered material demonstrated that the role of pyrite in the preservation of the Chengjiang Biota fossils may have been overestimated (Forchielli et al., 2014). Instead, carbonaceous films comprise the major original component of preservation in the Chengjiang Biota, and only some soft tissues were selectively replaced by pyrite (Edgecombe et al., 2015). However, C was lost in outcrop fossils probably due to the extensive activity of recent weathering (Gabbott et al., 2004; Gaines et al., 2008), as it is likely the case for the Fezouata Shale.

6. Conclusions

In this study, detailed sedimentological facies identified in the Fezouata Shale based on fresh core material offer unique insights into the mechanisms at play in the exceptional preservation. Distal environments of the Fezouata Shale below the SWB were inhabitable by living individuals. Dead organisms were exposed to pre-burial decay. At time of burial, based on observations of minimal bioturbation in the core, permissive anoxic conditions were established few cm below surface sediments. Under these conditions, pyrite replicated selectively some soft tissues, while the rest remained carbonaceous. Carbonaceous parts were then flattened due to compaction while pyrite replicates kept their 3D morphology. Afterward, carbon was leached from 2D compressions and surface sediments due to recent weathering. This weathering altered the original chemical signal of pyrite transforming it to iron oxides. When extensive weathering occurred, Mn and Co-rich deposits precipitated in addition to some star-shaped iron oxides that have nothing to do with the original anatomy of the fossils.

Acknowledgments

This paper is a contribution to the TelluS-Syster project ‘Vers de nouvelles découvertes de gisements à préservation exceptionnelle dans l’Ordovicien du Maroc’ (2017) and the TelluS-INTERRVIE projects ‘Mécanismes de préservation exceptionnelle dans la Formation des Fezouata’ (2018) and ‘Géochimie d'un *Lagerstätte* de l'Ordovicien inférieur du Maroc’ (2019), all funded by the INSU (Institut National des Sciences de l'Univers, France), CNRS. This paper is also a contribution to the International Geoscience Programme (IGCP) Project 653 – The onset of the Great Ordovician Biodiversification Event. The Raman facility in Lyon (France) is supported by the INSU. The authors thank Yves Candela, Lukáš Laibl, Eric Monceret, Martina Nohejlová, Stephen Pates, and Daniel Vizcaïno for assistance during field work in Montagne Noire or Morocco. The authors also thank Lukáš Laibl, Lorenzo Lustri, Fransesco Perez Peris, Claude Colombié and Gilles Montagnac for assistance during XRF, SEM and Raman spectroscopy analyses. Allison Daley is also thanked for facilitating access to the Fezouata Shale collections in Lausanne. Brian Pratt and all anonymous reviewers are also thanked for their constructive reviews on earlier versions of the manuscript.

Appendix A. Supplementary information

Supplementary information (including Table S1 and S2) associated with this article can be found, in the online version, at:

References

Ahm, A.-S.C., Bjerrum, C.J., Hammarlund, E.U., 2017. Disentangling the record of diagenesis, local redox conditions, and global seawater chemistry during the latest Ordovician glaciation. Earth and Planetary Science Letters 459, 145–156.

Anderson, R.P., Tosca, N.J., Gaines, R.R., Mongiardino Koch, N., Briggs, D.E.G., 2018. A mineralogical signature for Burgess Shale–type fossilization. Geology 46, 347–350.

Botting, J.P., 2016. Diversity and ecology of sponges in the Early Ordovician Fezouata Biota, Morocco. Palaeogeography Palaeoclimatology Palaeoecology 460, 75–86.

Butler, I.B., Rickard, D., 2000. Framboidal pyrite formation via the oxidation of iron (II) monoslfide by hydrogen sulphide. Geochimica et Cosmochimica Acta 64, 2665–2672.

Butterfield, N.J., 1995. Secular distribution of Burgess-Shale-type preservation. Lethaia 28, 1–13.

Caron, J.B., Scheltema, A., Schander, C., Rudkin, D., 2006. A soft-bodied mollusc with radula from the Middle Cambrian Burgess Shale. Nature 442, 159–163.

Caron, J.-B., Conway Morris, S., Shu, D., 2010. Tentaculate fossils from the Cambrian of Canada (British Columbia) and China (Yunnan) interpreted as primitive deuterostomes. PLoS One 5, e9586.

Choubert, G., 1952. Histoire géologique du domaine de l'Anti-Atlas. Géologie Internationale, 3e Série, Maroc.

Destombes, J., Hollard, H., Willefert, S., 1985. Lower Palaeozoic rocks of Morocco. In: Holland, C. (Ed.), Lower Palaeozoic Rocks of the World, pp. 91–336.

Duan, Y., Han, J., Fu, D., Zhang, X., Yang, X., Komiya, T., Shu, D., 2014. Reproductive strategy of the bradoriid arthropod *Kunmingella douvillei* from the Lower Cambrian Chengjiang Lagerstätte, South China. Gondwana Research 25, 983–990.

Edgecombe, G.D., Ma, X., Strausfeld, N.J., 2015. Unlocking the early fossil record of the arthropod central nervous system. Philosophical Transaction of Royal Society B: Biological Sciences 370, 20150038.

Fan, D., Liu, T., Ye, J., 1992. The process of formation of manganese carbonate deposits hosted in black shale series. Economic Geology 87, 1419–1429.

Farrell, Ú.C., 2014. Pyritization of soft tissues in the fossil record: an overview. The Paleontological Society Papers 20, a35-a58.

Forchielli, A., Kasbohm, J., Hu, S., Keupp, H., 2014. Taphonomic traits of clay-hosted early Cambrian Burgess Shale-type fossil Lagerstätten in South China. Palaeogeography Palaeoclimatology Palaeoecology 398, 59–85.

Gabbott, S.E., Xian-guang, H., Norry, M.J., Siveter, D.J., 2004. Preservation of Early Cambrian animals of the Chengjiang biota. Geology 32, 901-904.

Gaines, R.R., 2014. Burgess Shale-type preservation and its distribution in space and time. Paleontological Society Papers 20, 123–146.

Gaines, R.R., Briggs, D.E.G., Yuanlong, Z., 2008. Cambrian Burgess Shale–type deposits share a common mode of fossilization. Geology 36, 755-758.

Gaines, R.R., Briggs, D.E.G., Orr, P.J., Van Roy, P., 2012a. Preservation of giant anomalocaridids in silica-chlorite concretions from the Early Ordovician of Morocco. Palaios 27, 317–325.

Gaines, R.R., Hammarlund, E.U., Hou, X., Qi, C., Gabbott, S.E., Zhao, Y., Peng, J., Canfield, D.E., 2012b. Mechanism for Burgess Shale-type preservation. Proceedings of the National Academy of Science, USA 109, 5180–5184.

Grimes, S.T., Davies, K.L., Butler, I.B., Brock, F., Edwards, D., Rickard, D., Briggs, D.E.G., Parkes, R.J., 2002. Fossil plants from the Eocene London Clay: the use of pyrite textures to determine the mechanism of pyritization. Journal of the Geological Society of London 159, 493–501.

Gutiérrez-Marco, J.C., García-Bellido, D.C., 2015. Micrometric detail in palaeoscolecid worms from Late Ordovician sandstones of the Tafilalt Konservat-Lagerstätte, Morocco. Gondwana Research 28, 875–881.

Gutiérrez-Marco, J.C., García-Bellido, D.C., Rábano, I., Sá, A.A., 2017. Digestive and appendicular soft parts, with behavioural implications, in a large Ordovician trilobite from the Fezouata Lagerstätte, Morocco. Scientific Reports 7, 39728.

Hammer, Ø., Harper, D.A.T., Ryan, P.D., 2001. Past: paleontological statistics software package for education and data analysis. Palaeontologica Electronica 4, 4, 9p.

Harms, J.C., Southard, J.B., Spearing, D.R., Walker, R.G., 1975. Depositional environments as interpreted from primary sedimentary structures and stratification sequences. SEPM Short Course 2.

Jørgensen, B.B., 1982. Mineralization of organic matter in the sea bed – the role of sulphate reduction. Nature 296, 643–645.

Jørgensen, B.B., Findlay, A.J., Pellerin, A., 2019. The Biogeochemical Sulfur Cycle of Marine Sediments. Frontiers in Microbiology 10, 849.

Knaust, D., Desrochers, A., 2019. Exceptionally preserved soft-bodied assemblage in Ordovician carbonates of Anticosti Island, eastern Canada. Gondwana Research 71, 117–128.

Kouketsu, Y., Mizukami, T., Mori, H., Endo, S., Aoya, M., Hara, H., Nakamura, D., Wallis, S., 2014. A new approach to develop the Raman carbonaceous material geothermometer for low-grade metamorphism using peak width. Island Arc 23, 33–50.

Larsen, F., Postma, D., 1997. Nickel mobilization in a groundwater well field: release by pyrite oxidation and desorption from manganese oxides. Environmental Science and Technology 31, 2589–2595.

Lefebvre, B., Lerosey-Aubril R., Servais T., Van Roy, P., 2016. The Fezouata Biota: an exceptional window on the Cambro-Ordovician faunal transition. Palaeogeography Palaeoclimatology Palaeoecology 460, 1–6.

Lefebvre, B., Gutiérrez-Marco, J.C., Lehnert, O., Martin, E.L.O., Nowak, H., Akodad, M., El Hariri, K., Servais, T., 2018. Age calibration of the Lower Ordovician Fezouata Lagerstätte, Morocco. Lethaia 51, 296–311.

Lefebvre, B., Guensburg, T.E., Martin, E.L.O., Mooi, R., Nardin, E., Nohejlová, M., Saleh, F., Kouraïss, K., El Hariri, K., David, B., 2019. Exceptionally preserved soft parts in fossils from the Lower Ordovician of Morocco clarify stylophoran affinities within basal deuterostomes. Geobios 52, 27–36.

Lei, Q.-P., Han, J., Ou, Q., Wan, X.-Q., 2014. Sedentary habits of Anthozoa-like animals in the Chengjiang Lagerstätte: adaptive strategies for Phanerozoic-style soft substrates. Gondwana Research 25, 966–974.

Lerosey-Aubril, R., Paterson, J.R., Gibb, S., Chatterton, B.D.E., 2017. Exceptionally-preserved late Cambrian fossils from the McKay Group (British Columbia, Canada) and the evolution of tagmosis in aglaspidid arthropods. Gondwana Research 42, 264–279.

Liu, J., Shu, D., Han, J., Zhang, Z., Zhang, X., 2008. Origin, diversification, and relationships of Cambrian lobopods. Gondwana Research 14, 277–283.

Lucas, V., 2019. Mécanismes de préservation et étude géochimique de la carotte 18MFBI du Lagerstatte des Fezouata (Ordovicien inférieur, Maroc). M.Sc. Thesis, Brest University (unpubl.).

Martí Mus, M., 2016. A hyolithid with preserved soft parts from the Ordovician Fezouata Konservat-Lagerstätte of Morocco. Palaeogeography Palaeoclimatology Palaeoecology 460, 122–129.

Martin, E.L.O., Pittet, B., Gutiérrez-Marco, J.-C., Vannier, J., El Hariri, K., Lerosey-Aubril, R., Masrour, M., Nowak, H., Servais, T., Vandenbroucke, T.R.A., Van Roy, P., Vaucher, R., Lefebvre, B., 2016. The Lower Ordovician Fezouata Konservat-Lagerstätte from Morocco: age, environment and evolutionary perspectives. Gondwana Research 34, 274–283.

McKenzie, R., 1980. The adsorption of lead and other heavy metals on oxides of manganese and iron. Australian Journal of Soil Research 18, 61–73.

McMahon, S., Anderson, R.P., Saupe, E.E., Briggs, D.E.G., 2016. Experimental evidence that clay inhibits bacterial decomposers: Implications for preservation of organic fossils. Geology 44, 867–870.

Moysiuk, J., Smith, M.R., Caron, J.-B., 2017. Hyoliths are Palaeozoic lophophorates. Nature 541, 394–397.

Postma, D., 1985. Concentration of Mn and separation from Fe in sediments – I. Kinetics and stoichiometry of the reaction between birnessite and dissolved Fe(II) at 10°C. Geochimica et Cosmochimica Acta 49, 1023–1033.

Potter, R.M., Rossman, G.R., 1979. The manganese- and iron-oxide mineralogy of desert varnish. Chemical Geology 25, 79–94.

Rahl, J.M., Anderson, K.M., Brandon, M.T., Fassoulas, C., 2005. Raman spectroscopic carbonaceous material thermometry of low-grade metamorphic rocks: Calibration and application to tectonic exhumation in Crete, Greece. Earth and Planetary Science Letters 240, 339–354.

Raiswell, R., Whaler, K., Dean, S., Coleman, M., Briggs, D.E.G., 1993. A simple three-dimensional model of diffusion-with-precipitation applied to localised pyrite formation in framboids, fossils and detrital iron minerals. Marine Geology 113, 89–100.

Richard, D., Sundby, B., Mucci, A., 2013. Kinetics of manganese adsorption, desorption, and oxidation in coastal marine sediments. Limnology and Oceanography 58, 987–996.

Rickard, D., Luther, G.W., 1997. Kinetics of pyrite formation by the H2S oxidation of iron (II) monosulfide in aqueous solutions between 25 and 125°C: The mechanism. Geochimica et Cosmochimica Acta 61, 135–147.

Ruiz, G.M.H., Helg, U., Negro, F., Adatte, T., Burkhard, M., 2008. Illite crystallinity patterns in the Anti-Atlas of Morocco. Swiss Journal of Geosciences 101, 387–395.

Saleh, F., Candela, Y., Harper, D.A.T., Polechovà, M., Pittet, B., Lefebvre, B., 2018. Storm-induced community dynamics in the Fezouata Biota (Lower Ordovician, Morocco). Palaios 33, 535–541.

Saleh, F., Pittet, B., Perrillat, J., Lefebvre, B., 2019. Orbital control on exceptional fossil preservation. Geology 47, 103-106.

Saleh, F., Antcliffe, J.B., Lefebvre, B., Pittet, B., Laibl, L., Perez Peris, F., Lustri, L., Gueriau, P., Daley, A.C., 2020. Taphonomic bias in exceptionally preserved biotas. Earth and Planetary Science Letters 529, 115873.

Schiffbauer, J.D., Xiao, S., Cai, Y., Wallace, A.F., Hua, H., Hunter, J., Xu, H., Peng, Y., Kaufman, A.J., 2014. A unifying model for Neoproterozoic–Palaeozoic exceptional fossil preservation through pyritization and carbonaceous compression. Nature Communications 5, 5754.

Smith, M.R., Caron, J.-B., 2010. Primitive soft-bodied cephalopods from the Cambrian. Nature 465, 469–472.

Tang, D., Shi, X., Jiang, G., Zhou, X., Shi, Q., 2017. Ferruginous seawater facilitates the transformation of glauconite to chamosite: An example from the Mesoproterozoic Xiamaling Formation of North China. American Mineralogist 102, 2317–2332.

Topper, T.P., Greco, F., Hofmann, A., Beeby, A., Harper, D.A.T., 2018. Characterization of kerogenous films and taphonomic modes of the Sirius Passet Lagerstätte, Greenland. Geology 46, 359–362.

Torsvik, T., Cocks, L., 2011. The Palaeozoic palaeogeography of central Gondwana. Geological Society London Special Publications 357, 137–166.

Torsvik, T., Cocks, L., 2013. New global palaeogeographical reconstructions for the Early Palaeozoic and their generation. Geological Society London Memoirs 38, 5–24.

Van Roy, P., Orr, P.J., Botting, J.P., Muir, L.A., Vinther, J., Lefebvre, B., El Hariri, K., Briggs, D.E.G., 2010. Ordovician faunas of Burgess Shale type. Nature 465, 215–218.

Van Roy, P., Briggs, D.E.G., Gaines, R.R., 2015a. The Fezouata fossils of Morocco; an extraordinary record of marine life in the Early Ordovician. Journal of the Geological Society of London 172, 541–549.

Van Roy, P., Daley, A.C., Briggs, D.E.G., 2015b. Anomalocaridid trunk limb homology revealed by a giant filter-feeder with paired flaps. Nature 522, 77–80.

Vaucher, R., Martin, E.L.O., Hormière, H., Pittet, B., 2016. A genetic link between Konzentrat- and Konservat-Lagerstätten in the Fezouata Shale (Lower Ordovician, Morocco). Palaeogeography Palaeoclimatology Palaeoecology 460, 24–34.

Vaucher, R., Pittet, B., Hormière, H., Martin, E.L.O., Lefebvre, B., 2017. A wave-dominated, tide-modulated model for the Lower Ordovician of the Anti-Atlas, Morocco. Sedimentology 64, 777–807.

Vinther, J., Van Roy, P., Briggs, D.E.G., 2008. Machaeridians are Palaeozoic armoured annelids. Nature 451, 185–188.

Vinther, J., Parry, L., Briggs, D.E.G., Van Roy, P., 2017. Ancestral morphology of crown-group molluscs revealed by a new Ordovician stem aculiferan. Nature 542, 471–474.

Warner, N., Lgourna, Z., Bouchaou, L., Boutaleb, S., Tagma, T., Hsaissoune, M., Vengosh, A., 2013. Integration of geochemical and isotopic tracers for elucidating water sources and salinization of shallow aquifers in the sub-Saharan Drâa Basin, Morocco. Applied Geochemistry 34, 140–151.

Zhang, X., Liu, W., Zhao, Y., 2008. Cambrian Burgess Shale-type Lagerstätten in South China: distribution and significance. Gondwana Research 14, 255–262.

Zhu, M., Babcock, L.E., Steiner, M., 2005. Fossilization modes in the Chengjiang Lagerstätte (Cambrian of China): testing the roles of organic preservation and diagenetic alteration in exceptional preservation. Palaeogeography Palaeoclimatology Palaeoecology 220, 31–46.

Table and Figure captions

Table 1. Definition and associated depositional environment of outcrop facies (defined as F1, F2, and F4 in Vaucher et al., 2017) and core facies (defined as Fc1 to Fc5 in this study).

Fig. 1. Bou Izargane in the Ternata plain, Zagora area, Morocco. **A**. Paleographical location. **B**. Current location in the Ternata plain (30°30'00.5" N; 5°50'56.7" W).

Fig. 2. Sedimentary succession in the Fezouata Shale with a focus on the succession in Bou Izargane showing the alternation of thin background siltstones with coarse siltstone- to thin sandstone-dominated event levels. The positions of the drilled cores are indicated next to the sedimentary succession. The question marks in the stratigraphic column indicate intervals where characteristic graptolite assemblages could not be identified (Lefebvre et al., 2018).

Fig. 3. X-Ray Fluorescence maps of slightly altered core sediments of Fc3 at 405 cm (**A**), and non-altered deposits showing elemental distributions in Fc2 at 15 cm and Fc4 at 65 cm (**B**, **C**). Si is abundant in event beds that are normally graded (i.e., NGB). Al and K are positively correlated in background sediments. Fe and S are partially correlated in sediments highlighting the presence of pyrite minerals. S most probably indicates organic matter when it is not correlated to Fe. In slightly altered deposits, Mn and Co coexist in coarse sediments bearing sometimes Ca-rich bioclasts. Scale bars: 10 mm (A, B), 5 mm (C).

Fig. 4. **A**. Quartz-rich normally graded bedding (NGB) in the core alternating with clay-rich background sediments seen in thin section from sediments at 240 cm. **B**. Pyrite crystals (Py) in the fresh sediments surrounded by a halo of organic material (Om) at 250 cm. Pyrite and organic matter were identified based on Raman Spectra in Fig. 6. **C**. Bioclasts (Bioc) possibly of trilobite fragments from sediments at 262 cm. Scale bars: 5 mm (A), 1 mm (B, C).

Fig. 5. X-Ray Florescence maps of altered green core sediments of an intermediate Fc3-Fc4 facies at 1320 cm. These sediments show the absence of S-rich materials, except in the bottom part of the slab.

Mn and Co are enriched in these sediments in comparison with fresh material in Fig. 3(B, C). Scale bar: 5 mm.

Fig. 6. Raman spectra on thin sections (for analyzed material see Table S1, Appendix A) showing the presence of both pyrite and C in fresh core sediments, as well as the replacement of pyrite by iron oxides and the absence of organic C in weathered surface core slabs. The Raman spectra on organic material show the characteristic peaks of C.

Fig. 7. Facies evolution over the Bou Izargane succession. Most of normally graded beds are discontinuous due to bioturbation. Hummocky cross stratifications occur in the coarsest event deposits. Bioturbation is randomly distributed in the cores.

Fig. 8. Lithology in the Fezouata Shale. **A**. Quartz grain size evolution in Fc1to Fc5 seen in thin section with crossed-polarized light and λ/4 gypsum plate. **B**. Quantifying the increase of quartz content (SiO_2) and decrease of clay content (Al_2O_3, K_2O) (likely illite) between Fc1 and Fc5 (shown in A). Scale bars: 150 µm (Fc1), 200 µm (Fc2), 300 µm (Fc3), 400 µm (Fc4), and 400 µm (Fc5).

Fig. 9. Sedimentary structures in Fc1 (**A**), Fc2 (**B**), Fc3 (**C**), Fc4 (**D, E**) and Fc5 (**F**). Normally graded beds are frequently discontinuous due to bioturbation in B-F. Scale bars: 5 mm.

Fig. 10. Statistical analyses performed on facies evolution along the core from Bou Izargane. **A**. Principal Component Analysis of the 22, 60 cm-thick intervals defined along the core. **B**. Classical (hierarchical) Cluster Analysis of the 22 intervals according to Fc2, Fc3, and Fc4 distributions in these intervals. **C**. Similarity Percentage (Simper) analysis showing which facies are responsible for the differences between Cluster 1 and Cluster 2. **D**. Facies evolution (Fc1 to Fc5 in this study) along the core, correlated to outcrop succession (F1, F2, F4 from Vaucher et al., 2017) and clusters 1 and 2 obtained from the cluster analysis. Intervals bearing thin layers with exceptional preservation of fossils on the field are shown in dark grey, whereas intervals that did not yield any exceptional preservation are in light grey. Intervals with or without iron availability are shown according to Saleh et al. (2019). A 95% fit is observed between the alternation of clusters and levels with and without exceptional preservation, indicating that this type of preservation is strongly correlated with the sedimentary facies.

Fig. 11. Preservation mode of fossils in the Fezouata Shale, evidenced by SEM-EDX point spectroscopy of surface samples using accelerating voltages from 5 to 15 kV in order to enhance signal from light elements (C, O) and to promote fluorescence of heavier elements such as transition metals (Fe) in 3D fossils (**A**) and matrix and fossil imprints (**B**). Analyzed regions are marked as pink circles in the sample photographs. Scale bars: 5 mm (A), 10 mm (B).

Fig. 12. A-G. SEM images of minerals in samples from the Fezouata Shale. Iron rich minerals in white (A), euhedral iron-oxides (B, C), framboidal iron-rich minerals (D), star-like iron oxides (E) in addition to rose-shaped mineral (isolated, F) and next to smaller star-like minerals (G). **H**. SEM spectra showing that the star-like minerals are iron oxides and the rose-shaped ones are rich in manganese. Scale bars: 1 mm (A), 5 μm (B, E-G), 10 μm (C, D).

Fig. 13. Elemental maps of an extensively altered marrellomorph arthropod, AA-BIZ31-OI-39. Red/orange zones of the analyzed fossil are iron rich. Iron is preserved as star-like iron oxides. Scale bar: 10 mm.

Fig. 14. Mechanism for soft part preservation in the Fezouata Shale (**A-F**), and recent weathering explaining the preservation state of fossils (**G**). A: Living organism on the sea floor; B: Dead organism starts to decay prior to burial; C: Anoxic conditions are established due to burial, at the base of storm events, H_2S forms in decaying carcasses; D: Pyrite precipitation in specific tissues while the rest remains as carbonaceous material; E: With time, a facies similar to Fc2 is observed, combining conditions for both the colonization of the environment by a benthic fauna and for the preservation of this fauna; F: With compaction, fossils were preserved as 2D C-rich films with occasionally 3D pyritization; G: Recent weathering effect removes C from the fossils and alters the chemical signal of pyrite.

Table 1.

	Description	Depositional setting
F1	Argillaceous siltstones with sparse intercalations of siltstones (mm-thick)	Below storm weather base
F2	Coarse siltstones with hummocky cross-stratification (HCS) of cm-scale wavelength	Above storm weather base
F4	Fine sandstones with centimetric to decametric HCS, the laminations are underlined by thin layers of coarser quartz grains	Below Fair weather base
Fc1	Homogenous, composed of argillaceous material	Below storm weather base
Fc2	Siltstones with normally graded beds separated by argillaceous material	Below storm weather base, more proximal than Fc1
Fc3	Siltstones with stacked normally graded beds	Around the storm weather base
Fc4	Siltstones with stacked normally graded beds and abundant HCS	Above the storm weather base
Fc5	Coarse siltstones/fine sandstones with abundant bioclasts	Below fair weather base

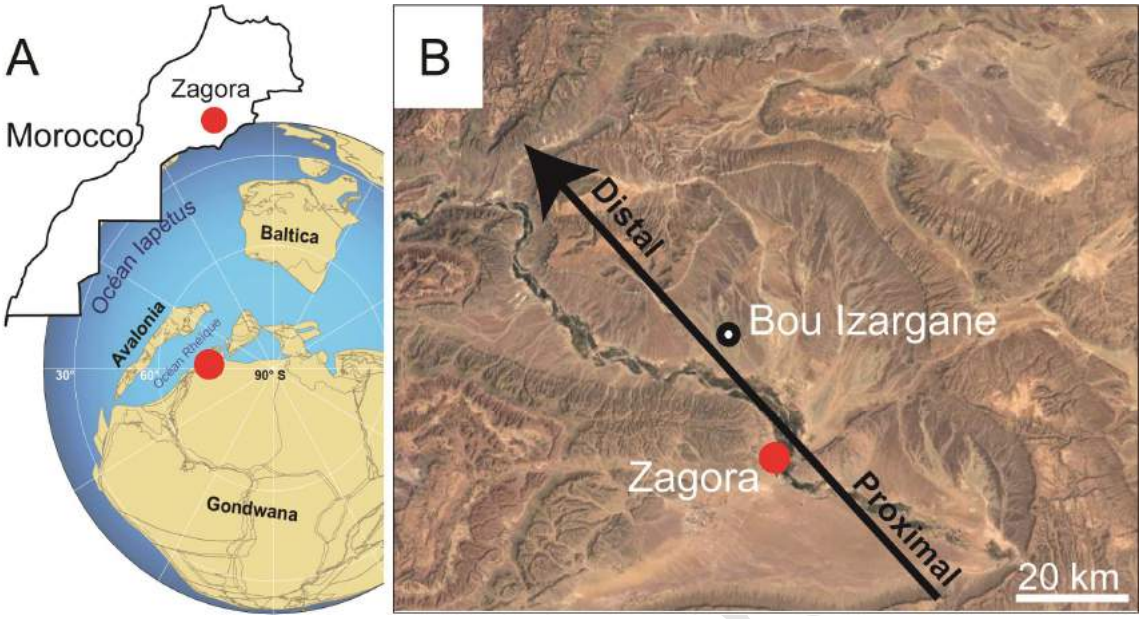

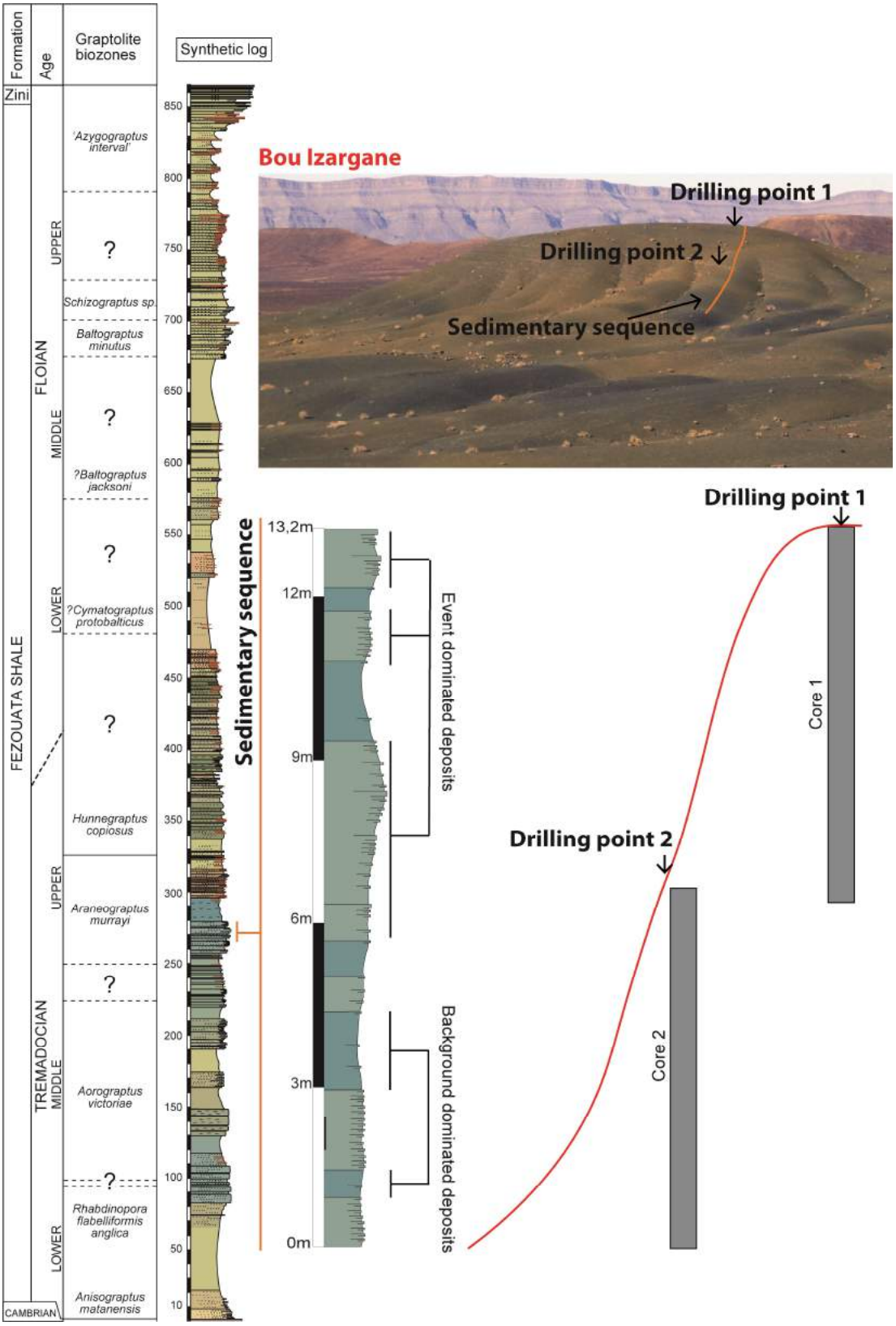
Formation
Age
Graptolite biozones
Synthetic log
Zini
FEZOUATA SHALE
FLOIAN
TREMADOCIAN
UPPER
MIDDLE
LOWER
CAMBRIAN
'Azygograptus interval'
?
Schizograptus sp.
Baltograptus minutus
?Baltograptus jacksoni
?Cymatograptus protobalticus
Hunnegraptus copiosus
Araneograptus murrayi
Aorograptus victoriae
Rhabdinopora flabelliformis anglica
Anisograptus matanensis
850
800
750
700
650
600
550
500
450
400
350
300
250
200
150
100
50
10
Bou Izargane
Drilling point 1
Drilling point 2
Sedimentary sequence
Sedimentary sequence
13,2m
12m
9m
6m
3m
0m
Event dominated deposits
Background dominated deposits
Drilling point 1
Drilling point 2
Core 1
Core 2

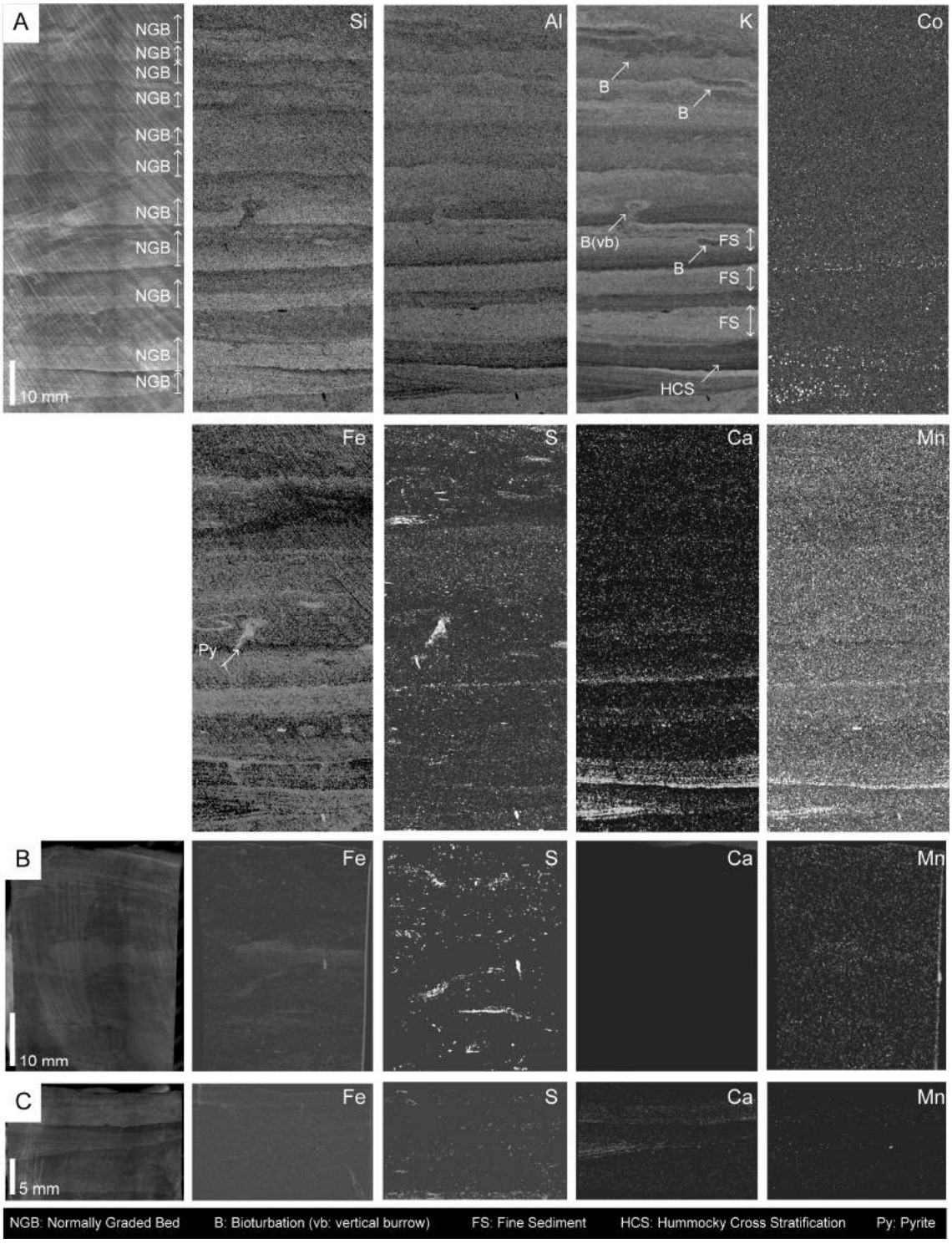
A
NGB
NGB
NGB
NGB
NGB
NGB
NGB
NGB
NGB
NGB
10 mm
Si
Al
K
B
B
B(vb)
B
FS
FS
FS
HCS
Co
Fe
Py
S
Ca
Mn
B
10 mm
Fe
S
Ca
Mn
C
5 mm
Fe
S
Ca
Mn
NGB: Normally Graded Bed
B: Bioturbation (vb: vertical burrow)
FS: Fine Sediment
HCS: Hummocky Cross Stratification
Py: Pyrite

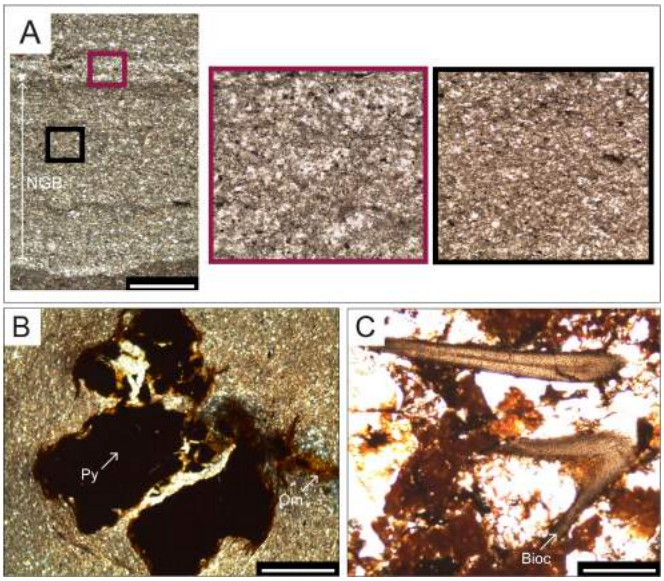

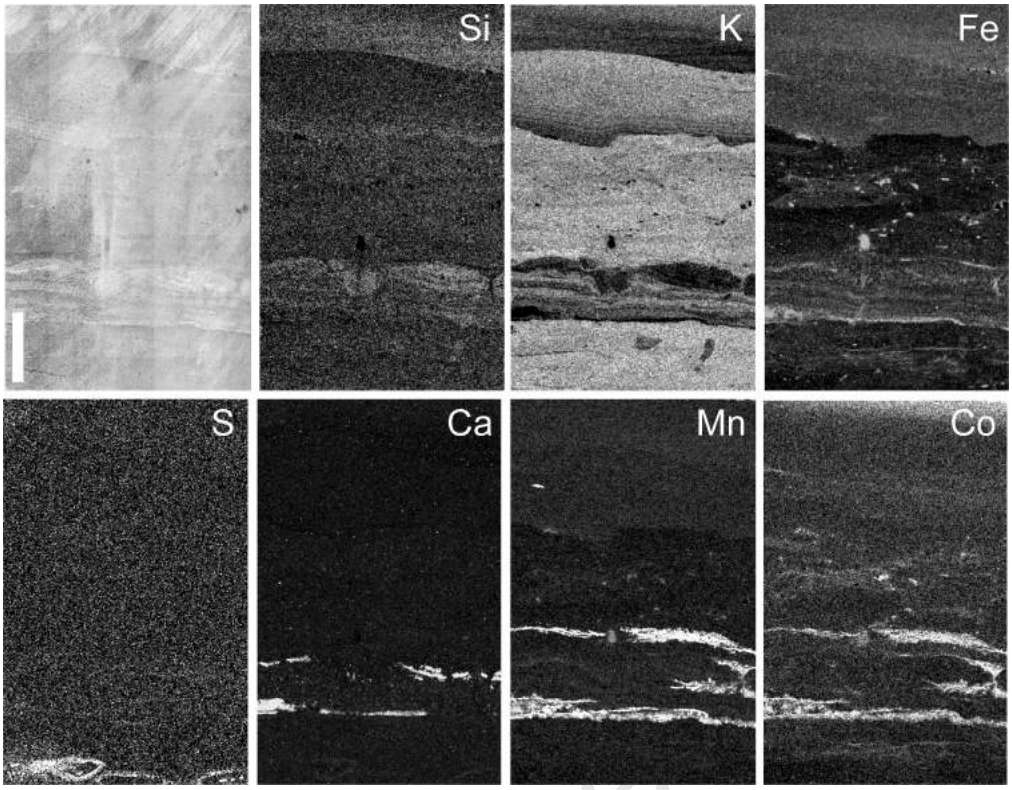

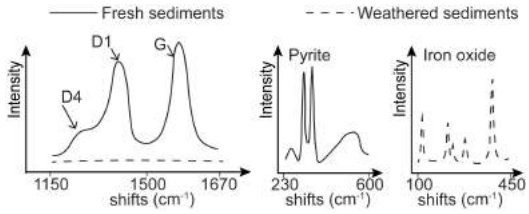


Facies
0m
1m
2m
3m
4m
5m
6m
7m
8m
9m
10m
11m
12m
13m
Siltstones
Coarse
Fine
Normal grading
Wavy laminations
Bioturbation
Bioclastic beds
Exceptional preservation (field outcrops)

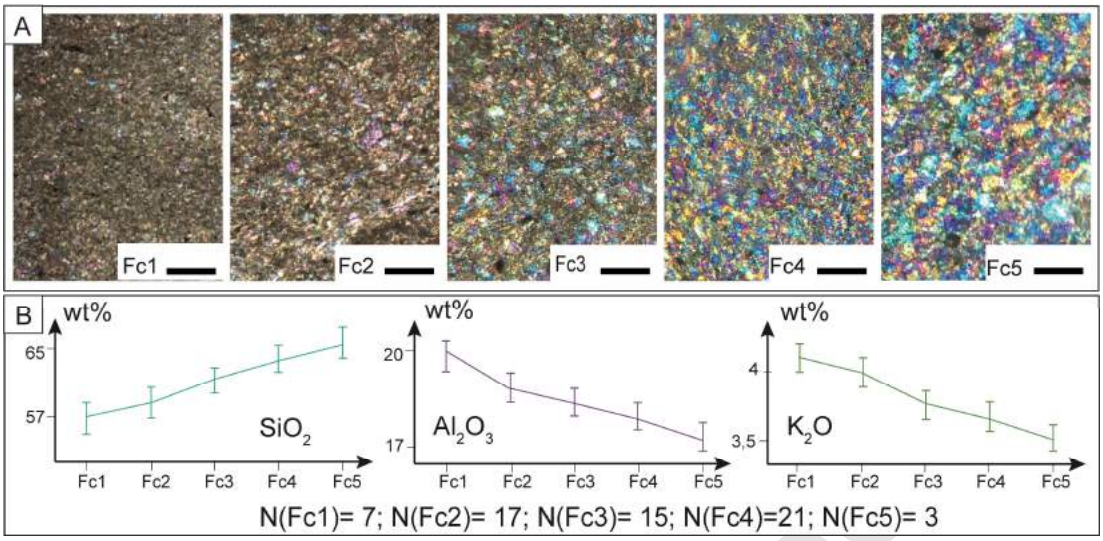

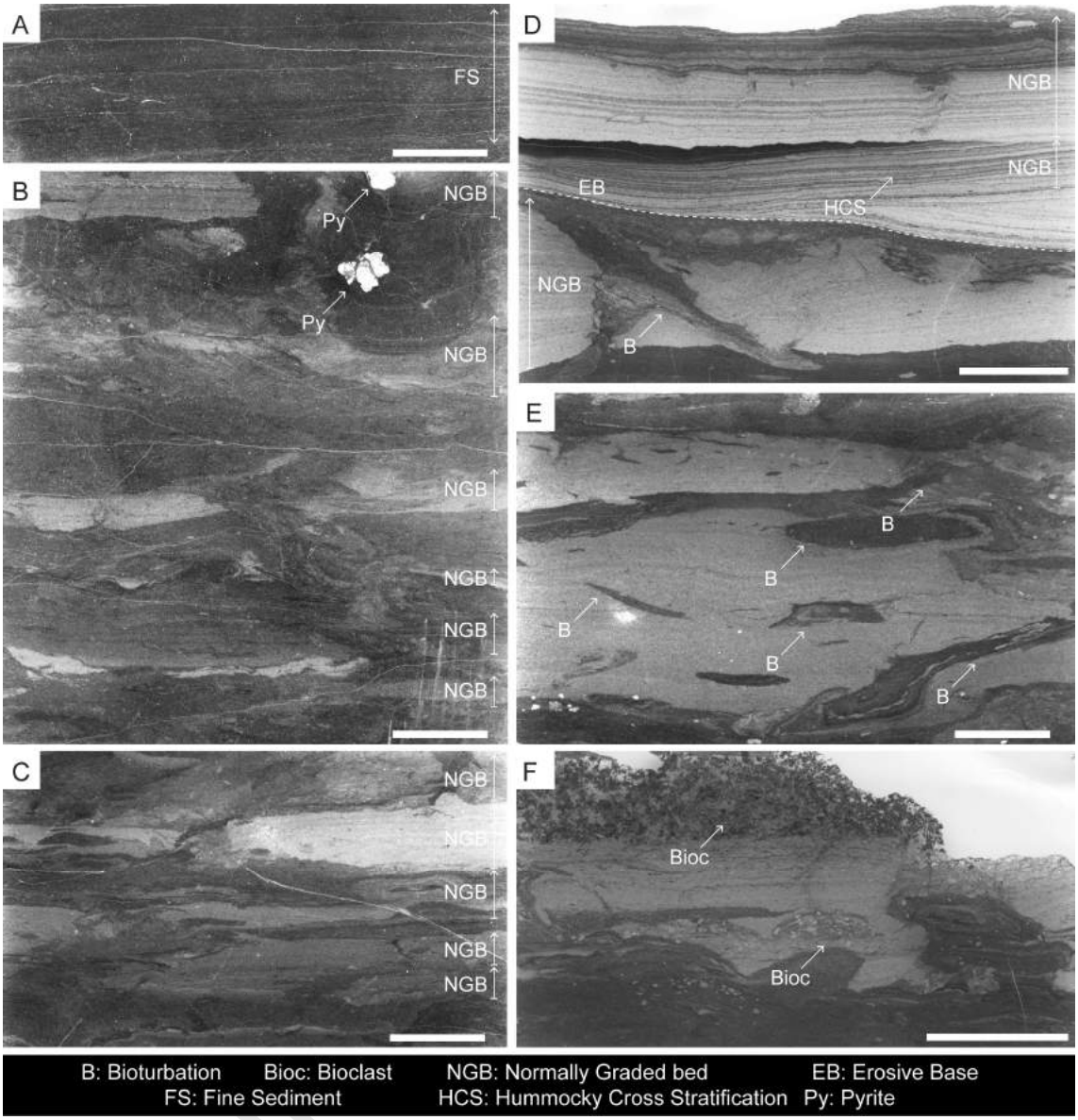

B: Bioturbation Bioc: Bioclast NGB: Normally Graded bed EB: Erosive Base
FS: Fine Sediment HCS: Hummocky Cross Stratification Py: Pyrite

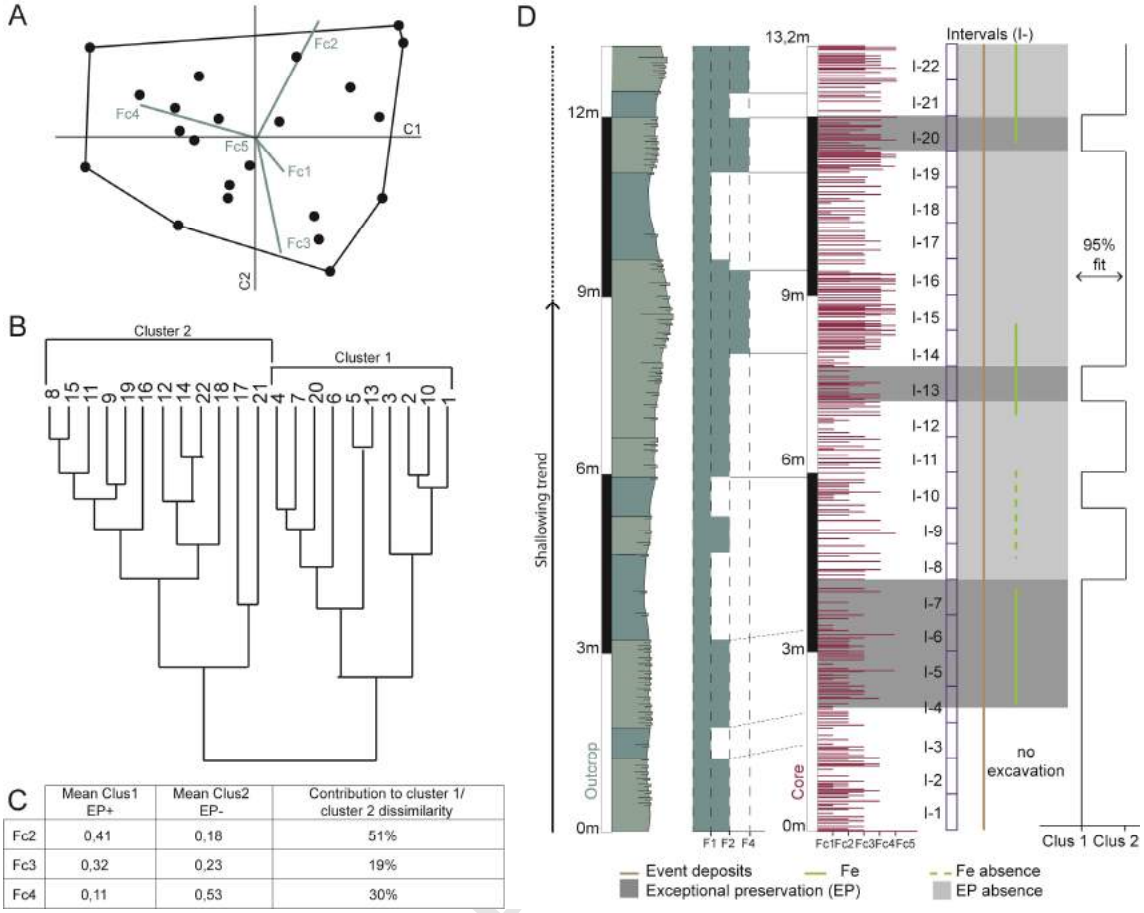

C

	Mean Clus1 EP+	Mean Clus2 EP-	Contribution to cluster 1/ cluster 2 dissimilarity
Fc2	0,41	0,18	51%
Fc3	0,32	0,23	19%
Fc4	0,11	0,53	30%

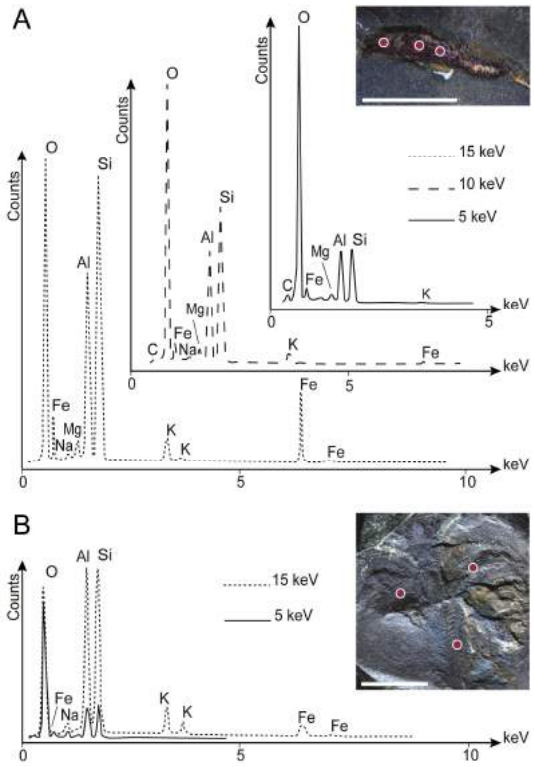

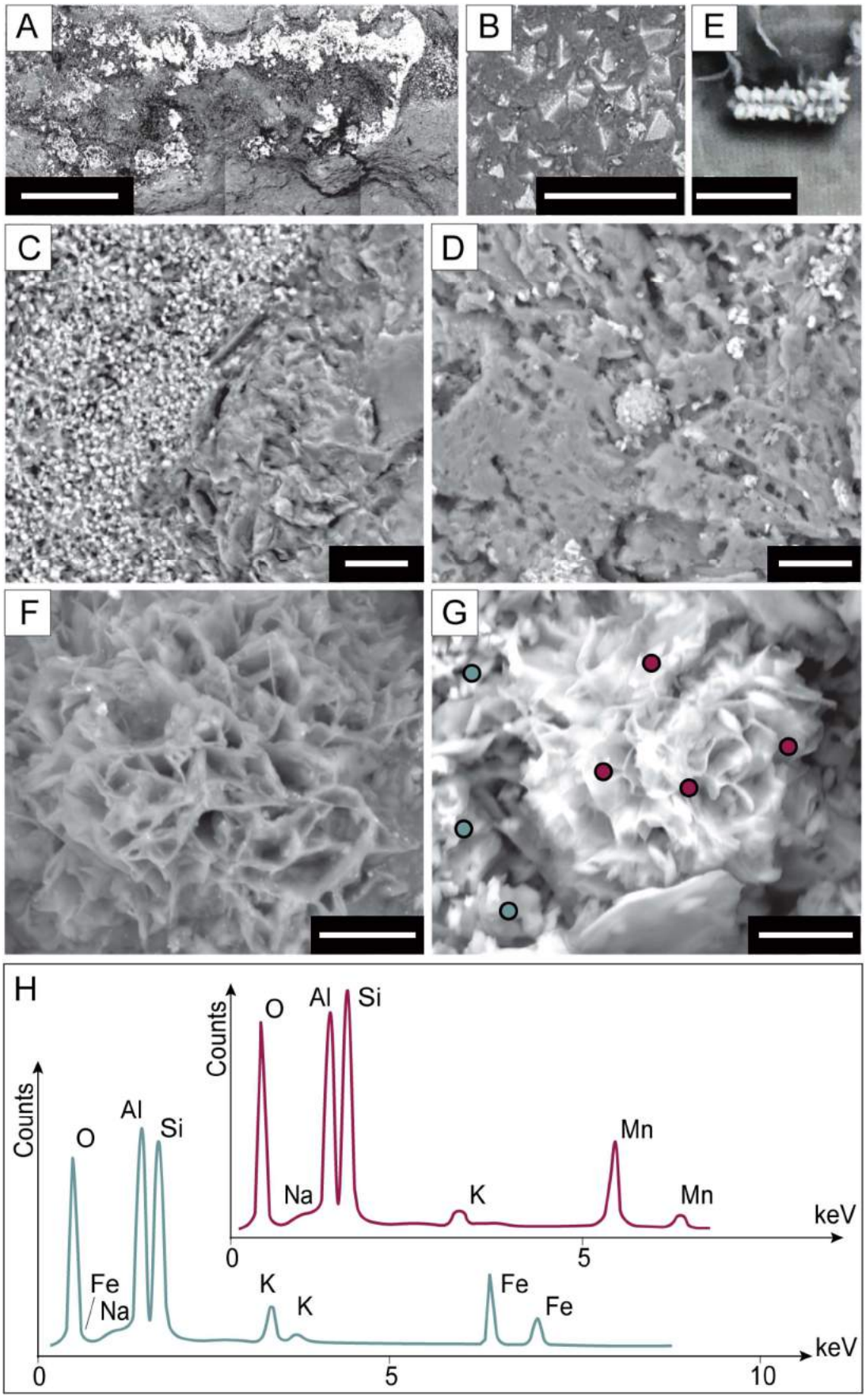
A
B
E
C
D
F
G
H
Counts
O
Al
Si
Fe
Na
K
K
Fe
Fe
0
5
10
keV
Counts
O
Al
Si
Na
K
Mn
Mn
0
5
keV